CHEMISTRY OF MATERIALS

ARTICLE

pubs.acs.org/cm

Thin Films of Ge−Sb−Te-Based Phase Change Materials: Microstructure and in Situ Transformation

Jan Tomforde and Wolfgang Bensch*

Institute of Inorganic Chemistry, Christian-Albrechts University, Max-Eyth-Str. 2, D-24118 Kiel, Germany

Lorenz Kienle

Institute for Materials Science, Synthesis and Real Structure, Christian-Albrechts University, Kaiserstrasse 2, D-24143 Kiel, Germany

Viola Duppel

Max Planck Institute for Solid State Research, Heisenbergstrasse 1, D-70569 Stuttgart, Germany

Philipp Merkelbach and Matthias Wuttig

RWTH Aachen University, I. Institute of Physics, 52056 Aachen, Germany

Supporting Information

ABSTRACT: The ternary compounds $GeSb_2Te_4$ and $Ge_2Sb_2Te_4$ are promising phase change materials for application in the fields of data storage and recording. In the present study, thin films of the materials were deposited on inert substrates using the magnetron sputter technique. The microstructures of the amorphous, metastable, and stable crystalline states were investigated by X-ray powder diffractometry and high resolution transmission electron microscopy (HRTEM). In the as-deposited state, the materials are amorphous. Upon heating, they crystallize first into a metastable phase with a NaCl-type structure, followed by a transformation into a layered structure (stable phase) at higher temperatures. HRTEM studies reveal that nanosized particles with a granular morphology are present in all materials for the crystalline metastable state. In the case of $GeSb_2Te_4$, these nanocrystals do not grow significantly when the sample transforms to the stable phase, which contains layers of structural vacancy. $Ge_2Sb_2Te_4$ behaves differently. In particular, the structural transition to the crystalline stable phase is accompanied by a pronounced increase in the crystallite size up to several micrometers. The crystals are built from nanoscale lamellae, which do not contain vacancy layers. Rietveld refinement of the X-ray data of $Ge_2Sb_2Te_4$ in the metastable crystalline state reveals that the compound consists of two phases of which one is Ge rich and the other Ge poor. The size of the coherent scattering domains in the former phase was about 20 nm, whereas the value for the second phase was determined to be about 2 nm.

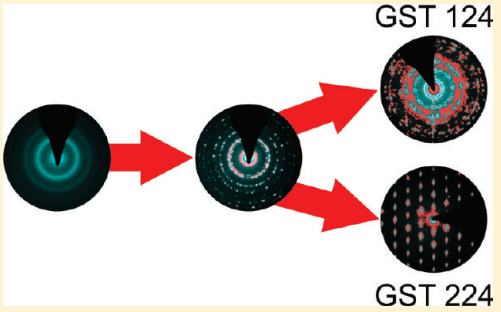

KEYWORDS: phase change materials, microstructure, phase transition, HRTEM

INTRODUCTION

Thin films of phase change materials (PCM) based on ternary Ge−Sb−Te (GST) alloys are of practical relevance because of their use in optical data storage devices like CDs, DVDs, and Blu-ray disks.[1] The crystallization and amorphization of PCMs leads to pronounced changes of the electronic and optical properties, which can be used to store, erase, and read information. Different chemical bonding appears as demanding criterion for the property changes upon phase change.[2] Only a subset of GSTs are assumed to exhibit the required properties for memory applications,[3] and most studies were performed on phases nGeTe•$m$$Sb_2Te_3$, e.g., $Ge_2Sb_2Te_5$ ("GST225" with n = 2; m = 1). Upon heating, thin films of GST225 first transform to a metastable NaCl-type structure (space group: $Fm\bar{3}m$) characterized by structural disordering of Ge/Sb atoms and intrinsic structural vacancies (20% per formula unit) on joint crystallographic sites. Depending on the measurement technique and film thickness, different crystallization temperatures (T_{c1}) were reported ranging from 140 to 175 °C.[4−8] For instance, in situ X-ray scattering experiments on GST225 films and nanoparticles[9] indicate no significant difference of T_{c1} (∼160 °C). Moreover, the speed of crystallization critically depends on film thickness,[10] and after repeated cycling, phase segregation was reported for GST225.[11] At more elevated temperatures (T_{c2} ∼ 300 °C), a second and

Received: March 23, 2011
Revised: July 11, 2011
Published: August 17, 2011

irreversible structural transition to a stable phase occurs.[12−15] The trigonal or rhombohedral structures of the GSTs are characterized by hexagonal layers of Ge/Sb, respectively Te atoms that are stacked similarly to the NaCl-type, but the slabs are separated by a van der Waals gap like in simple transition metal dichalcogenides, e.g., TiQ_2 (Q = S, Se, or Te). Such van der Waals gaps may be also described as vacancy layers (VL) due to missing (Ge/Sb) atoms on the cation positions of the rocksalt-type structure within this layer.[17] For the different compositions of Ge−Sb−Te-based PCMs, the number of stacked (Ge/Sb) and Te layers within the unit cell is different, and GST225 exhibits a nine-layer structure with the following stacking sequence: Te−(Ge,Sb)−Te−(Ge,Sb)−Te—Te−(Ge,Sb)−Te—(Ge,Sb),[16] whereas GST124 crystallizes with a 21-layer structure.[12] The separation between adjacent slabs varies characteristically for the distinct compositions of PCMs,[17] i.e., the widths of the VL are different for the different materials. An important observation is indicative that the phase transition from the metastable NaCl-type structure into the trigonal/rhombohedral structure is a first-order transition: the transition is accompanied by a discontinuity in the atomic volume.[12]

Besides conventional heating, electron beam irradiation can be applied for the initiation of structural ordering. In the case of a thermally transformed GST225 film (T = 130 °C), colonies with 400 nm diameters consisting of 10−20 nm sized grains were observed with TEM. In this study, crystallization of the material could be induced using a 400 kV electron beam. According to the results, nucleation is strongly promoted by the electron beam, but crystal growth seems to be unaffected.[18] Some local ordering of Ge and Sb on the cation site in the metastable NaCl-type structure was proposed on the basis of HRTEM studies performed on GST225 films.[19] In another HRTEM study on a GST225 film annealed at 200 °C, the coexistence of the metastable cubic phase and of the stable structure in one grain was postulated, suggesting that the material is in the process of the phase transformation at this temperature.[20] Doping of GST225 with In, Bi, or Sn maintains the metastable cubic phase but alters the transition temperature from the amorphous to crystalline state.[21]

The phase GST124 containing 25% intrinsic vacancies on the cation sublattice is much less examined than GST225. The crystallization temperature seems to be slightly lower than for GST225.[8] The X-ray powder pattern of GST124 films annealed between 120 and 160 °C exhibits only reflections of the metastable cubic phase.[22] TEM investigations together with the results of X-ray diffractometry show that cubic GST124 consists of grains with dimensions of 20−150 nm, which are formed by 2−15 nanocrystallites of dimensions between 9 and 11 nm. Increasing the annealing temperature leads to an increase in the grain sizes and an increase in the dimension and number of crystallites within the grains.[23] Using scanning tunnelling microscopy and spectroscopy, the transition temperature T_{c1} for GST124 was determined to be around 120 °C.[24] The second structural transition into the stable trigonal phase with a 21-layer structure in the unit cell is observed at about 200 °C.[12,22] The partial substitution of Te by Se in GST124 leads to a slight decrease in the first transition temperature and to a higher temperature for the transition into the stable structure.[25]

Besides the prominent PCM properties, these tellurides are also promising candidates for thermoelectric applications. For instance, Bi_2Te_3/Sb_2Te_3 superlattices[26] containing two constituents like the PCMs showed spectacular thermoelectric properties, and it is believed that nanostructuring of suitable materials may be introduced for a reduction of the lattice thermal conductivity via nanoscale phonon scattering centers.[27] The state of the art of the syntheses and characterization of thermoelectric materials was recently reviewed in several papers,[28] and rules for a reduction of the thermal conductivity were summarized: (i) scattering of the phonons within the unit cell by creating rattling structures or point defects such as interstitials, vacancies, or by alloying; (ii) use of complex crystal structures to separate the electron-crystal from the phonon-glass; and (iii) scattering of phonons at interfaces in multiphase composites on the nanoscale.

Interestingly, PCM materials show low thermal conductivities, which could be of interest for thermoelectric applications around room temperature, e.g., 0.2 W m^{-1} K^{-1} for amorphous GST-225.[29−32] For the cubic phase, the published data vary between 0.28 and 0.57 W m^{-1} K^{-1}, and for the trigonal phase, the data vary between 0.46 and 1.58 W m^{-1} K^{-1}.[29−32] The relatively large variation may be due to deviations from the stoichiometry or the formation of nanostructures during processing.[33]

According to the results presented above, GST124 and GST225 behave similarly; however, much less is known about $Ge_2Sb_2Te_4$ (GST224).[34,35] GST224 with a rocksalt-type structure contains no intrinsic structural vacancies; hence, a significant difference to the other GSTs is expected. It was proposed that GST224 should exhibit excellent optical contrast when switching between the amorphous and metastable crystalline states.[34] In several studies, it was shown that the instrinsic structural vacancies on the cationic sublattice are important for the stabilization and phase change properties of the materials.[14,34] Further stabilization stems from the half-filled p-band[20] of the alloys nGeTe•$m$$Sb_2Te_3$; however, GST224 has an average number of 3.25 p-electrons per atom. Hence, the p-band is more than half-filled, and on the basis of such a lack of stabilization, GST224 might not be a single-phase compound and may instead form a multiphase composite material. Moreover, applying the chemical rules and assuming Te to be present as Te^{2-} anions, charge compensation could only be achieved by unusual oxidation states for Ge and Sb or the formation of bonds between these two elements. Nevertheless, the X-ray powder diffraction pattern of a crystallized GST224 film suggested the formation of a single-phase material crystallizing in the metastable cubic structure.[35] Obviously, the structural properties of GST224 on different length scales are not clear, which motivated us to study GST224 in more detail. Such a study is of great importance in view of the very recently reported unusual electric behavior of GST124 and other PCMs. A GST124 film showed a transition from insulating to metallic charge upon annealing, which is explained by a disorder-induced metal-to-insulator transition caused by a change in charge−carrier mobility at almost constant charge−carrier density. The authors mentioned that control of the degree of disorder in the crystalline state is essential for the realization of multilevel resistance states. Such control would allow application in nonvolatile storage devices.[36] In this contribution, the results of in situ X-ray diffraction (XRD) experiments, Rietveld refinements, and high-resolution transmission electron microscopy (HRTEM) studies performed on the different structural states of GST124 and GST224 films are presented.

EXPERIMENTAL DETAILS

PCM films were deposited on clean substrates (Si wafers and glass) by dc magnetron sputtering from stoichiometric compound targets of near

bulk density produced by Umicore. The deposition on unheated substrates produced amorphous films. The background pressure was $\sim 10^{-6}$ mbar before the deposition, and the working pressure during power-controlled sputtering in Ar ambient was 7×10^{-3} mbar. The sputtering power was 20 W. Film thickness was determined with a profilometer on a reference sample to be 1 μm. For the powder X-ray measurements, the samples were deposited on glass substrates. They were scratched off prior to crystallization under Argon atmosphere. After deposition, in situ X-ray data was collected on a D8 Advance $\theta-\theta$ diffractometer (Cu Kα radiation, λ = 1.54056 Å) with a Göbel mirror and a reflectometry high-temperature chamber (MRI-HTC). The in situ experiments were performed under vacuum ($p < 10^{-5}$ mbar). The temperature was gradually increased in steps of 5 °C, with a heating rate of 0.1 K/sec and held constant during collection of XRD patterns.

Powder X-ray data for the Rietveld refinements were collected for the two materials GST124 and GST224 in the metastable state on beamline 2 at HASYLAB, DESY, Hamburg using λ = 0.49342 Å with the samples being placed in glass capillaries with a diameter of 0.3 mm. Because GST124 and GST224 in the stable state are less important as PCM, no high-resolution X-ray data were recorded. The background of the patterns was treated by interpolation of hand-selected points. The reflection profiles were modeled using either a pseudo-Voigt profile (one-phase refinement) or the Thompson−Cox−Hastings profile function in the program package FULLPROF.[37] A standard LaB_6 pattern measured on the same instrument was used as a resolution function file. For the one-phase refinement (GST124), Ge and Sb were equally distributed on the 4b site in space group $Fm\bar{3}m$. A two-phase refinement was necessary for GST224 restraining all B_{iso} values to a common value that was fixed at the early stages of refinement. The site occupancy factors (sof) of Ge and Sb were refined without restraints; however, after convergence was reached, they were fixed during further refinements. This procedure yields the compositions $Ge_{2.1}Sb_{1.2}Te_4$ and $Ge_{1.1}Sb_{2.6}Te_4$ for the two phases with an estimated ratio of 61(2):39(2) mol %.

Thin films were also evaporated onto copper grids that serve as supports for electron microscopy. The films were deposited from the same targets under identical deposition conditions. In a second series of experiments, fractions of the $GeSb_2Te_4$ and $Ge_2Sb_2Te_4$ films were annealed in a furnace ("ex situ heated", 2 h above T_c) and subsequently transferred to the grids. HRTEM was performed with a Philips CM 30ST (LaB_6 cathode, 300 kV, C_S = 1.15 mm). Selected area electron diffraction (SAED) was carried out using a diaphragm that limited the diffraction to a circular area of 2500 Å in diameter. All images were recorded with a CCD camera. Chemical analyses by EDX were performed in the nanoprobe mode or by spectral imaging (scanning mode) with a Si/Li detector (cf. also EDX spectra in the Supporting Information. Cliff−Lorimer k-factors (MBTS, no absorbance): 1.509 (Ge−K), 1.738 (Sb−L), 1.781 (Te−L)). To analyze structural transformations of the samples under the influence of the electron beam, two different exposure modes can be selected in the microscope, namely, a low-dose mode for observation ("observation mode") and a high-dose mode for transformation ("transformation mode"). The latter was adjusted by selecting higher emission parameters and removing the condenser aperture. The increase in current density of the transformation versus the observation mode was estimated to be 40-fold.

RESULTS AND DISCUSSION

The as-deposited and amorphous thin films with nominal compositions of GST124 and GST224 were examined via EDX nanoprobe analyses (TEM) and spectral imaging for the presence of nanoscale inhomogeneities. Both techniques show a fully homogeneous distribution of the elements as proven by the low variances of 1 atom % for the single point measurements. However, slight deviations from the nominal compositions were identified, with an atomic ratio of Ge:Sb:Te = 14(1):29(1):57(1) (average of eight point analyses, calculated atomic ratio of 13:32:55). The chemical homogeneity is well supported by the lack of any concentrations in the mass−thickness contrast of bright field images.

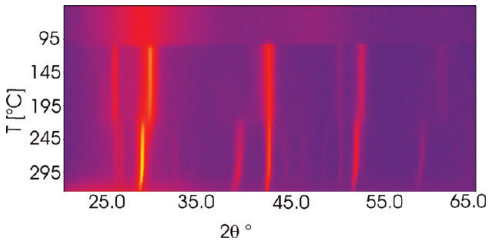

Figure 1. XRD pattern recorded on a GST124 thin film in the course of in situ heating.

In situ XRD scans of an initially amorphous GST124 film on a glass substrate show the transformation into the crystalline metastable state at T_{c1} = 127(2) °C ($Fm\bar{3}m$, a = 6.0250(3) Å) (Figure 1), which is near the value of 130 °C reported earlier using differential scanning calorimetry (DSC)[38,39] but is lower than the peak crystallization temperatures of 164.6 °C, respectively 145 °C given in refs 8 and 34 . The Rietveld refinement of the high-resolution powder pattern with FULLPROF using the profile of LaB_6 as the standard yields 21.3(0.2) nm and 32.0(1) ‰ for the apparent size and strain, respectively. The standard deviations given in the global average apparent size and strain are calculated using the different reciprocal lattice directions and are a measure of the degree of anisotropy, not of the estimated error.

At about 220 °C, a phase transition to the stable trigonal structure ($R\bar{3}m$, a = 4.23186(7) Å, c = 41.0675(1) Å; a = 4.21, c = 40.6 Å for $Ge_{0.94}Sb_2Te_4$[40]) occurs. The transition temperature T_{c2} is similar to those (200 and 215 °C) published in refs 38 and 39 using DSC and of ~200 °C determined with STM.[20,24] Note, that both transition temperatures are lower than those for GST225[6] with T_{c1} = 140−175 °C[4−8] and $T_{c2} \sim$ 300 °C.

HRTEM observations support the amorphous structure of the films, and consequently, the SAED patterns recorded on GST124 (Figure 2a, right) as well as Fourier transforms of high-resolution micrographs (not shown) display very broad and diffuse intensity on concentric rings. HRTEM micrographs prove the absence of any crystallinity on the nanoscale in the as-deposited material (Figure 2a, left). Such an amorphous structure is not changed for GST124 during HRTEM observations. However, when switching to transformation mode (Experimental Section), a characteristic development of structural ordering occurs.

A comparison of in situ transformed and ex situ annealed GST124 proved that the same microstructures were formed. On the basis of this finding, we propose that the in situ crystallization is mainly initiated from heating the samples by the electron beam impact. The latter is also indicated by the suppression or at least decreased rate of in situ transformation in areas with close contact to the heat-conducting copper grid. In the following, results based on in situ transformation are presented.

As demonstrated by the series of SAED patterns in panel (b) of Figure 2 (from left to right: t = 0, 30, 60 s), the diffuse intensity of the initially amorphous material concentrates with increasing time of irradiation in transformation mode. After 1 min, the pattern contains Bragg reflections on the well-resolved concentric rings (Figure 2c, right). Their diameters correlate

with the cubic structure of c-GST124 (d_{calc}/d_{exp} for rings 1−6 [Å]: $(111)_c$, 3.49/3.49; $(200)_c$, 3.02/3.05; $(220)_c$, 2.14/2.14; $(222)_c$, 1.74/1.74; $(400)_c$, 1.51/1.52; and $(420)_c$, 1.35/1.36).[12]

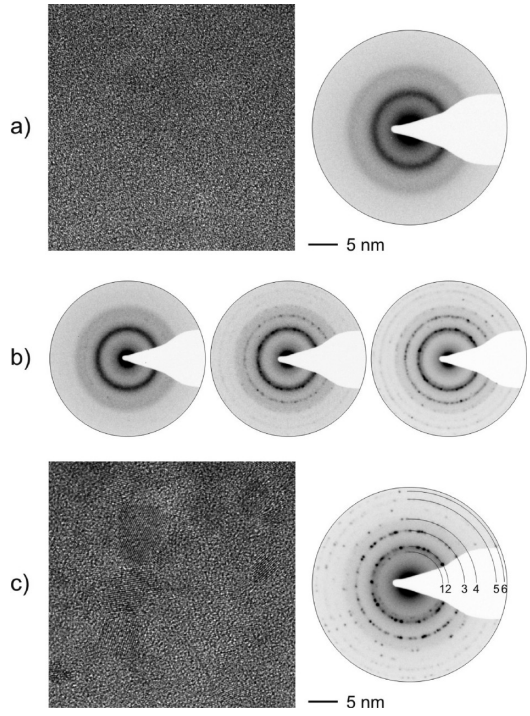

Figure 2. (a) HRTEM micrograph of as-deposited GST124 and SAED pattern. (b) Series of SAED patterns each recorded after switching to a high dose (transformation mode) for 30 s. (c) HRTEM micrograph (section of image a) after transformation by massive electron impact and corresponding SAED pattern.

The HRTEM micrograph in panel (c) of Figure 2 demonstrates that the initially formed cubic grains with average sizes up to 20 nm, being in good agreement with the size estimated from X-ray powder pattern, are rotationally disordered and are still embedded within an amorphous matrix. As expected for intermediates of glasses and crystals, their lattices are strongly distorted; hence, the diffracted intensity fades at high resolution. Extended times of irradiation just slightly increase the sizes of the grains, but their crystalline perfection is strongly enhanced and the structure inside the grains changes.

Following the analyses on annealed GST124[12], the cubic symmetry of the initial product is reduced to trigonal (index "t") by a structural phase transition. The interrelated ordering of the structure is associated with a pronounced arrangement of structural vacancies inside $(111)_c$ layers. In moderate underfocus and when aligned parallel to the zone axis, the VL are displayed as lines with bright dots in high resolution mode. This is demonstrated for the structure of GST124 (Figure 3a, arrows highlighting the VLs) by a selected simulated micrograph (Figure 3b) and the matrix of simulated micrographs in dependence of thickness and defocus (cf. Figure 3c).

Note that the orientation of VL with respect to the cubic structure is fixed by group−theoretical considerations. In particular, one of the $\{111\}_c$ layers must be aligned parallel to the basal layer of the trigonal system $(001)_t$, which is parallel to the VL.

After extended times of irradiation, diffraction patterns containing diffuse scattering with concentrations on positions $[111]^*_c/4$ can be observed (not shown). According to the cubic structure, the grains now contain domains with 4-fold unit-cell dimensions ($d(003)_t \sim 4 \times d(111)_c$) as expected for trigonal GST124, and the ordering is frequently disturbed. When adjusting grains close to the zone axis $[110]_c$, two sets of $(111)_c$ layers as possible VL are aligned parallel to the zone axis. Hence, VL

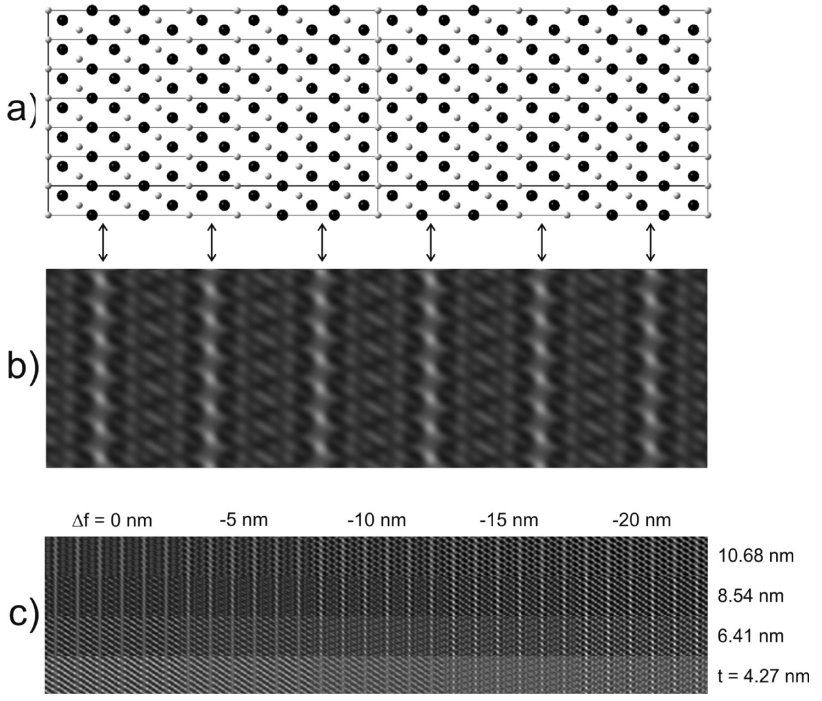

Figure 3. (a) Projection of the trigonal structure of GST124 along [100], (b) simulated micrograph ($\Delta f = -10$ nm, $t = 8.54$ nm), and (c) matrix of simulated micrographs for different thicknesses and defocus value.

dx.doi.org/10.1021/cm200835a |*Chem. Mater.* 2011, 23, 3871–3878

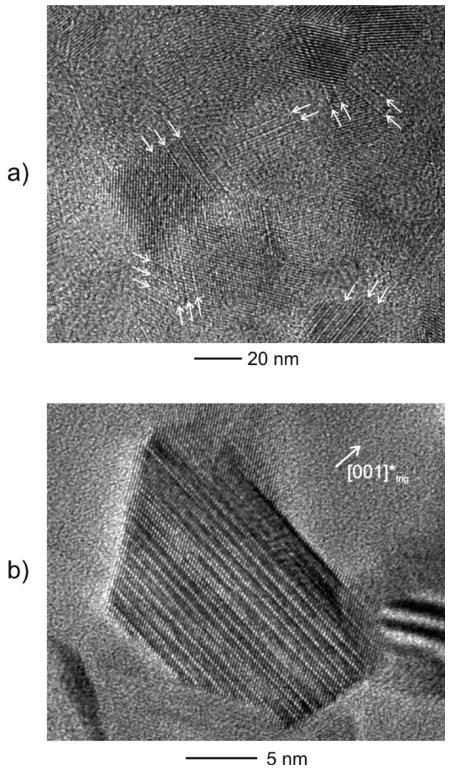

Figure 4. HRTEM micrographs of GST124 recorded after extended times of irradiation (transformation mode). (a) Rotationally disordered grains with VL. (b) Single grain with variable distances of the VL along $[001]^*_t$.

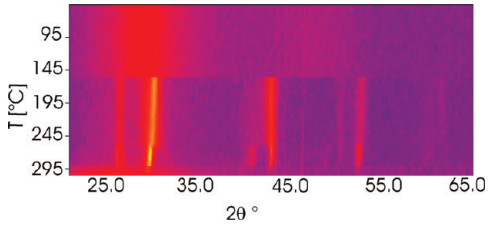

Figure 5. XRD pattern recorded on a GST224 thin film in the course of in situ heating.

formation can be easily identified for moderate underfocus, cf. lines containing bright spots in the micrograph of panel (a) of Figure 4. Like the cubic precursor, neighboring grains are rotationally disordered, and even inside the same grain the variable distances between the VL indicate layered disordering (Figure 4b).

For the Ge-richer GST224 film, the transition from amorphous to crystalline state occurs at about $T_{c1} = 150$ °C (Figure 5). At 265 °C, the NaCl-type structure shows a transition into a unknown structure as further evidenced by the HRTEM investigations (see below). It is clearly observed that the temperatures at which the phase changes take place differ significantly for GST224 and GST124.

A closer look onto the high-resolution X-ray powder pattern of c-GST224 at room temperature reveals that this material exhibits a more complex microstructure (Figure 6 top). All reflections show a shoulder on the low angle side, and some of the refined reflection positions do not match with the peak positions.

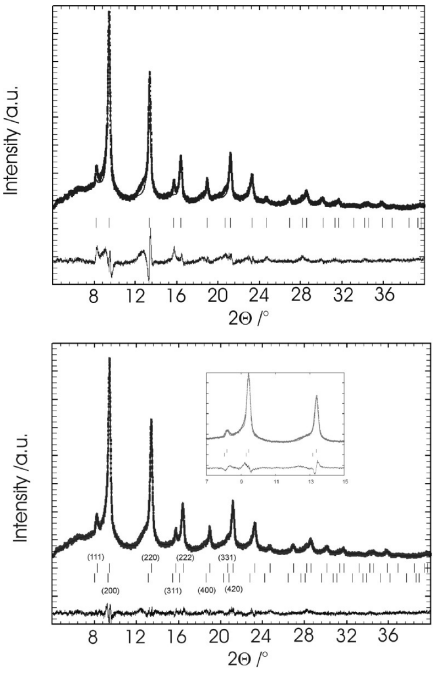

Figure 6. Results of the Rietveld refinements performed on c-GST224. Top: one-phase refinement; bottom: two-phase refinement (details see text). Points: experimental data. Line: calculated data. Vertical bars: Bragg positions (top row: $Ge_{2.1}Sb_{1.2}Te_4$; bottom row: $Ge_{1.1}Sb_{2.6}Te_4$). Bottom trace: difference between calculated and experimental data. Some of the reflections are indexed. Inset shows an enlarged view of a Rietveld refinement without shift of the reflections.

Moreover, several reflection intensities are not well reproduced with the structural model applied (see difference plot in Figure 6 top). These observations are hints for the coexistence of two phases with similar lattice parameters (cf. shoulders), the presence of stacking faults and/or antiphase domains (shift of reflection positions), and different sizes of the coherent scattering domains. The Rietveld refinements based on two cubic phases with different chemical compositions $Ge_{2.1}Sb_{1.2}Te_4$ for phase I and $Ge_{1.1}Sb_{2.6}Te_4$ for phase II yield a refined ratio of 61(2):39(2) (Experimental Section). During the structure refinement, the calculated positions of some reflections of $Ge_{2.1}Sb_{1.2}Te_4$ (phase I) do not match with the measured positions, particularly for the (111), (220), and (620) reflections (Figure 6 bottom, inset). Hence, the positions of these reflections were allowed to shift individually. Despite the individual shifting of the reflections, the agreement between calculated and measured reflection profiles was not satisfactory. Therefore, a size broadening of reflections was also introduced that affected the series of reflections $(h + k + l) = 2n$ and which further increased the agreement between calculated and measured reflection profiles. The low values of the reliability factors and the good agreement of calculated and measured X-ray data suggest that the model chosen adequately reproduces the experimental data (Figure 6 bottom). It is quite interesting that both stoichiometries found in the GST224 film have structural vacancies on the Ge/Sb sublattice. Their presence confirms that vacancies indeed stabilize the crystalline lattice of the PCMs discussed here.[29] Another interesting result is the remarkable difference of the reflection widths of the two phases. Using the Scherrer formula (no correction for instrumental broadening), the average size of

Table 1. Results of Rietveld Refinement for the One-Phase (1) and Two-Phase Refinements (2)[a]

	1	2	
a (Å)	5.9964(7)	5.9940(2)	6.1100(1)
χ^2	41.3	15.3	
R_{Bragg} (%)	11.4	4.41	7.99

[a] Estimated standard deviations are given in parentheses.

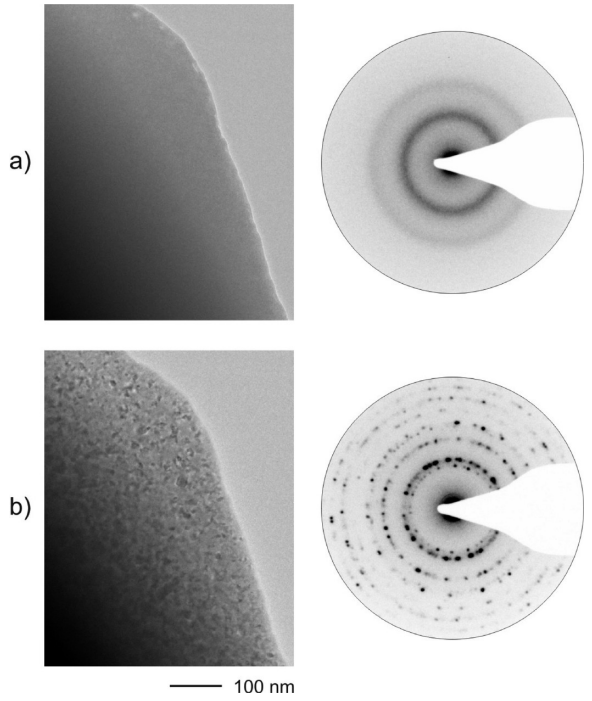

Figure 7. Bright field images and SAED patterns recorded on GST224 before (a) and after step I of the in situ transformation (b).

coherent scattering crystallites is about 20 nm for phase I and 2 nm for phase II. The apparent size and strain was also calculated with FULLPROF using the profile of LaB_6 as the standard. This analysis yields 44.5(16.9) nm and 65.4(1) ‰, respectively, for phase I (the meaning of the standard deviation is explained above). For phase II, no strain is observed, and the apparent size is 1.55(1) nm. The lattice parameters of the two phases differ by about 0.11 Å (Table 1), which can be explained by the different compositions. In phase II, the Sb content is much larger than in phase I, and the covalent radius of Sb is larger than that of Ge, leading to the observed difference. We note that in the powder pattern of GST224 reported in[35] the (200) and (220) reflections also show a shoulder on the low angle side, of which no further comments were made.

The bright field images and SAED patterns of as-deposited GST224 films verify the fully amorphous structure and chemical homogeneity (Figure 7a) before in situ transformation. EDX measurements indicate no segregation as verified by the low variances for single-point measurements (atomic ratio of Ge:Sb:Te = 24(1):28(1):48(1), average of six point analyses, calculated ratio of 25:25:50). Like for GST124, a comparative study of in situ transformed and conventionally annealed films confirms that related real structures are formed. However, the scenario of

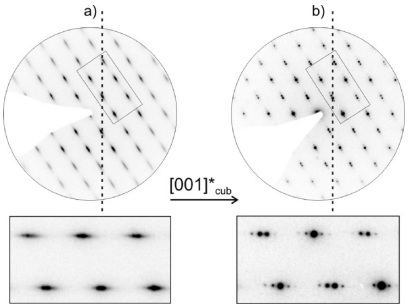

Figure 8. SAED patterns (top) recorded in two distinct selected areas (a and b) of GST224 after the second transformation with enlarged sections (bottom).

crystallization and structural changes is unique. Two steps of transformation can be separated.

In analogy to GST124, the first step transformation produces crystalline grains with average sizes below 20 nm, as evidenced by the spots in the bright field contrast of panel (b) of Figure 7, left. The attached SAED pattern can be indexed assuming a cubic *F*-centered structure with lattice parameter $a \sim 6.0(1)$ Å. In contrast to c-GST124, the crystallization of cubic grains can hardly be avoided even in the observation mode, suggesting a much more pronounced beam-sensitivity of as deposited GST224 compared to GST124. Because of the limited spatial resolution of the applied microscope in scanning mode, the EDX analyses indicate no phase separation after the initial crystallization. When switching to the transformation mode (see above and the Experimental Section), a second in situ transformation occurs. The characteristic grain structure of c-GST224 disappears immediately, and extended crystalline areas with sizes of several micrometers are formed. In contrast to all other PCMs, this transformation proceeds even outside the directly transmitted area and is linked with a strong deformation of the films. Extended irradiation with high doses does not initiate further changes of the real structure. The SAED patterns of distinct zone axes orientations clearly reflect the single grain but composite nature of the films. With the restriction to main structure reflections, the patterns could be approximated by assuming a simple NaCl-type structure model ($Fm\bar{3}m$, $a \sim 6$ Å). However, a closer inspection reveals significant violations of the cubic symmetry, as shown in Figure 9 for areas aligned close to a zone axis orientation correlating with $[110]_c$.

The metrics deviate significantly from rectangularity, e.g., the angle between the directions specified as $[001]^*_c$ and $[-110]^*_c$ (see arrow and vertical broken lines in Figure 8, respectively). Such a distortion accounts for a symmetry reduction from the cubic (*F*-centered) to a trigonal (*R*-centered) average structure, e.g., space group $R\bar{3}m$ and lattice parameters deviating from the ideal values of $a \sim 4.24$ Å and $c \sim 10.39$ Å (hexagonal setting). Moreover, locally varying intensity between the main structure reflections indicates a complexity of the real structure beyond a simple NaCl-type model. This is highlighted by diffuse streaks (Figure 8a) and their concentration into satellite reflections at noninteger positions of reciprocal space, cf. formation of an incommensurate structure (Figure 8b). As expected for the trigonal system, the streaks are extended along $[001]^*_t$. The HRTEM investigation proves that these phenomena depend on a specific nanostructure that is not based on VL formation like for GST124. The films consist of well-separated $(001)_t$ lamellae with

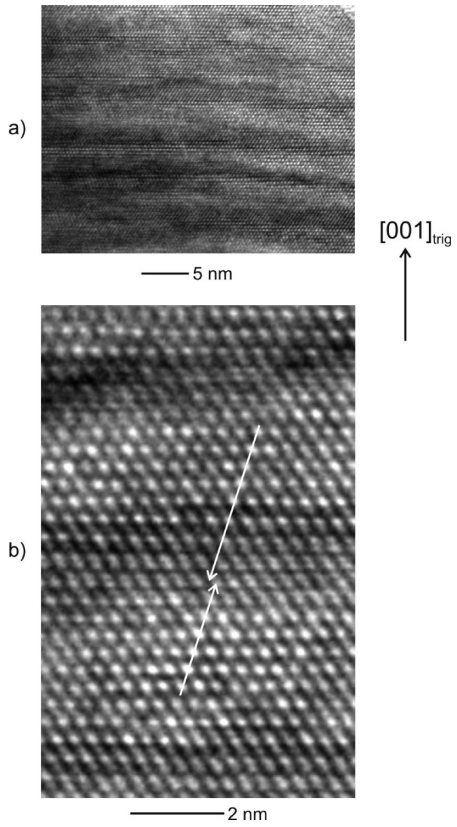

Figure 9. (a) HRTEM micrograph of the lamellar nanostructure of GST224 after second transformation, zone axis orientation $[100]_t$. (b) Magnified view of the boundary region between two lamellae.

an average thickness below 20 nm, cf. the horizontal stripes of panel (a) of Figure 9. The Fourier transforms calculated inside circular cutouts of single lamellae do not show significant differences of the lattice parameters. Nanoprobe EDX analyses revealed that the average composition remains unchanged during the transformation. However, the compositions of the single lamellae could not be determined due to the limitations of spatial resolution.

The separation of the lamellae is based on a shift (see arrows in Figure 9b), allowing an interpretation of the lamellae in terms of nanoscale antiphase domains. The boundaries between adjacent lamellae appear as stripes perpendicular to $[001]_t$. At the boundary between two lamellae, HRTEM micrographs display a superposition phenomenon, e.g., for zone axis $[100]_t$ (Figure 9b) by a splitting of the single bright spots into double spots. Depending on the periodicity of the nanostructure along $[001]_t$, the distinct scattering phenomena like satellites and streaks are produced. In particular, the rule case of a nonperiodic sequence of $(001)_t$ lamellae with distinct thicknesses produces the diffuse streaks along $[001]^*_t$.

SUMMARY

The microstructures of the different states of GST124 and GST224 (amorphous, metastable, stable) were characterized on different length scales by a combined approach of XRD and HRTEM. Both samples are amorphous in the as-deposited state and undergo two-phase transitions upon heating. For both samples, a granular structure is formed after the transition into the metastable NaCl-type phase. According to the X-ray investigations, GST224 contains two different phases in the metastable state, i.e., a Ge-rich and a Sb-rich phase coexist. These two phases exhibit significantly different sizes for the nanocrystals with the Ge-rich phase being roughly 10 times larger than the Ge-poor phase. For the second transition, a pronounced difference of the PCMs was identified. GST124 shows the formation of VL inside the grains, while for GST224, large crystals are obtained that do not show VL but antiphase domains.

ASSOCIATED CONTENT

Supporting Information. EDX spectra of the samples in different stages. This information is available free of charge via the Internet at http://pubs.acs.org/.

AUTHOR INFORMATION

Corresponding Author

*E-mail: wbensch@ac.uni-kiel.de. Tel: +49 431 880-2419. Fax: +49 431 880-1520.

ACKNOWLEDGMENT

The authors thank Prof. Dr. Dr. h. c. mult. A. Simon for his continuing support. Financial support by the DFG (priority program SPP1386), BE 1653/18-2 and Wu 243/18-2 is gratefully acknowledged. L.K. thanks the DFG for Grant KI 1263/4-1. We also thank DESY (Hamburg) for beamtime allocation.

REFERENCES

(1) (a) Wuttig, M; Yamada, N. *Nat. Mater.* **2007**, *6*, 824. (b) Bensch, W.; Wuttig, M. *Chemie Unserer Zeit* **2010**, *2*, 82. (c) Wuttig, M. *Nat. Mater.* **2005**, *4*, 265. (d) Raoux, S.; Wełnic, W.; Ielmini, D. *Chem. Rev.* **2010**, *110*, 240. (e) Gille, T.; De Meyer, K.; Wouters, D. J. *Phase Trans.* **2009**, *81*, 773. (f) Welnic, W.; Wuttig, M. *Mater. Today* **2008**, *11*, 20. (g) Kolobov, A. V.; Fons, P.; Tominaga, J. *Thin Solid Films* **2007**, *515*, 7534. (h) Wuttig, M.; Steimer, C. *Appl. Phys.* **2007**, *A 87*, 411.

(2) Shportko, K.; Kremers, S.; Woda, M.; Lencer, D.; Robertson, J.; Wuttig, M. *Nat. Mater.* **2008**, *7*, 653.

(3) Lencer, D; Salinga, M.; Grabowski, B.; Hickel, T.; Neugebauer, J.; Wuttig, M. *Nat. Mater.* **2008**, *7*, 972.

(4) Park, J.; Kim, M. R.; Choi, W. S.; Seo, H.; Yeon, C. *Jpn. J. Appl. Phys.* **1999**, *38*, 47775.

(5) Seo, H.; Jeong, T.-H.; Park, J. W.; Yeon, C.; Kim, S.-J.; Kim, S.-Y. *Jpn. J. Appl. Phys.* **2000**, *39*, 745.

(6) Friedrich, I.; Weidenhof, V.; Njoroge, W.; Franz, P.; Wuttig, M. *J. Appl. Phys.* **2000**, *87*, 4130.

(7) Privitera, S.; Rimini, E.; Bongiorno, C.; Zonca, R.; Pirovano, A.; Bez, R. *J. Appl. Phys.* **2003**, *94*, 4409.

(8) Kalb, J. A.; Wuttig, M.; Spaepen, F. *J. Mater. Res.* **2007**, *22*, 748.

(9) Raoux, S.; Rettner, C. T.; Jordan-Sweet, J. L.; Kellock, A. J.; Topuria, T.; Rice Dolores, P. M.; Miller, C. *J. Appl. Phys.* **2007**, *102*, 094305.

(10) Martens, H. C. F.; Vlutters, R.; Prangsma, J. C. *J. Appl. Phys.* **2004**, *95*, 3977.

(11) Raoux, S.; Shelby, R. M.; Jordan-Sweet, J.; Munoz, B.; Salinga, M.; Chen, Y.-C.; Shih, Y.-H.; Lai, E.-K.; Lee, M.-H. *Microelectron. Eng.* **2008**, *85*, 2330.

(12) Matsunaga, T.; Yamada, N. *Phys. Rev. B* **2004**, *69*, 104111.

(13) Sun, Z.; Zhou, J.; Ahuja, R. *Phys. Rev. Lett.* **2006**, *96*, 055507.

(14) Matsunaga, T.; Kojima, R.; Yamada, N.; Kifune, K.; Kubota, Y.; Tabata, Y.; Takata, M. *Inorg. Chem.* **2006**, *45*, 2235.

(15) Kooi, B. J.; De Hosson, J; Th., M. *J. Appl. Phys.* **2002**, *92*, 3584.

(16) Matsunaga, T.; Yamada, N.; Kubota, Y. *Acta Crystallogr. B* **2004**, *60*, 685.

(17) Schürmann, U.; Duppel, V.; Buller, S.; Bensch, W.; Kienle, L. *Cryst. Res. Technol.* **2011**, DOI: DOI: 10.1002/crat.201000516.
(18) Kooi, B. J.; Groot, W. M. G.; De Hosson, J; Th., M. *J. Appl. Phys.* **2004**, *95*, 924.
(19) Park, Y. J.; Lee, J. Y.; Youm, M. S.; Kim, Y. T.; Lee, H. S. *J. Appl. Phys.* **2005**, *97*, 093506–1.
(20) Sun, C.; Lee, J.; Kim, Y. *Phys. Stat. Solidi A* **2009**, *206*, 50.
(21) Wang, K.; Steimer, C.; Wamwangi, D.; Ziegler, S.; Wuttig, M.; Tomforde, J.; Bensch, W. *Microsyst Technol.* **2007**, *13*, 203.
(22) Fuxi, G.; Songsheng, X.; Zhengxiu, F. *Ann. Phys.* **1992**, *1*, 391.
(23) Prokhorov, E.; Trapaga, G.; González-Hernández, J. *J. Appl. Phys.* **2008**, *104*, 103712.
(24) Subramaniam, D.; Pauly, C.; Liebmann, M.; Woda, M.; Rausch, P.; Merkelbach, P.; Wuttig, M.; Morgenstern, M. *Appl. Phys. Lett.* **2009**, *95*, 103110.
(25) Tomforde, J.; Buller, S.; Ried, M.; Bensch, W.; Wamwangi, D.; Heidelmann, M.; Wuttig, M. *Solid State Sci.* **2009**, *11*, 683.
(26) Venkatasubramanian, R.; Siivola, E.; Colpitts, T.; O'Quinn, B. *Nature* **2001**, *413*, 597.
(27) Rao, M.; Ji, X.; Tritt, T. M. *MRS Bull.* **2006**, *31*, 218.
(28) Snyder, G. J.; Toberer, E. S. *Nat. Mater.* **2008**, *7*, 105. Tritt, T. M.; Subramanian, M. A. *MRS Bull.* **2006**, *31*, 188. Tritt, T. M. *Phys. Stat. Sol. (RRL)* **2007**, *1*, A91. Sommerlatte, J.; Nielsch, K.; Böttner, H. *Phys. J.* **2007**, *6*, 35. Böttner, H.; Chen, G.; Venkatasubramanian, R. *MRS Bull.* **2006**, *31*, 211. Nolas, G. S.; Poon, J.; Kanatzidis, M. G. *MRS Bull.* **2006**, *31*, 199. Vining, C. B. *Nat. Mater.* **2009**, *8*, 83. Vineis, C. J.; Shakouri, A.; Majumdar, A.; Kanatzidis, M. G. *Adv. Mater.* **2010**, *22*, 3970.
(29) Kim, E. K.; Kwun, S. I.; Lee, S. M.; Seo, H.; Yoon, J. G. *Appl. Phys. Lett.* **2000**, *76*, 3864.
(30) Peng, C.; Cheng, L.; Mansuripur, M. *J. Appl. Phys.* **1997**, *82*, 4183.
(31) Giraud, V.; Cluzel, J.; Sousa, V.; Jacquot, A.; Dauscher, A.; Lenoir, B.; Scherrer, H.; Romer, S. *J. Appl. Phys.* **2005**, *98*, 013520.
(32) Lyeo, H.-K.; Cahill, D. G.; Lee, B.-S.; Abelson, J. R.; Kwon, M.-H.; Kim, K.-B.; Bishop, S. G.; Cheong, B.-K. *Appl. Phys. Lett.* **2006**, *89*, 151904.
(33) Poudel, B.; Hao, Q.; Ma, Y.; Lan, Y.; Minnich, A.; Yu, B.; Yan, X.; Wang, D.; Muto, A.; Vashaee, D.; Chen, X.; Liu, J.; Dresselhaus, M. S.; Chen, G.; Ren, Z. *Science* **2008**, *320*, 634.
(34) (a) Wuttig, M.; Lüsebrink, D.; Wamwangi, D.; Wełnic, W.; Gillessen, M.; Dronskowski, R. *Nat. Mater.* **2007**, *6*, 122. (b) Da Silva, J. L. F.; Walsh, A.; Wei, S.-H.; Lee, H. *J. Appl. Phys.* **2009**, *106*, 113509. (c) Matsunaga, T.; Kojima, R.; Yamada, N.; Kifune, K.; Kubota, Y.; Takata, M. *Chem. Mater.* **2008**, *20*, 5750.
(35) Wełnic, W.; Kalb, J. A.; Wamwangi, D.; Steimer, C.; Wuttig, M. *J. Mater. Res.* **2007**, *22*, 2368.
(36) Siegrist, T.; Jost, P.; Volker, H.; Woda, M.; Merkelbach, P.; Schlockermann, C.; Wuttig, M. *Nat. Mater.* **2011**, *10*, 202.
(37) Rodriguez-Carvajal, J.; Roisnel, T. *FULLPROF2k*; Rietveld, March 2009.
(38) Yamada, N.; Ohno, E.; Nishiuchi, K.; Akahira, N.; Takao, M. *J. Appl. Phys.* **1991**, *69*, 2849.
(39) (a) Yamada, N.; Ohno, E.; Akahira, N.; Nishiuchi, K.; Nagata, K.; Takao, M. *Proc. Int. Symp. Optical Memory* **1987**, *26*, 61. (b) *Jpn. J. Appl. Phys.* **1987**, *26* (Suppl.), 26–4.
(40) Karpinsky, O. G.; Shelimova, L. E.; Kretova, M. A.; Fleurial, J.-P. *J. Alloys Compd.* **1998**, *268*, 112.